STATUS OF THE CERN SYNCHROCYCLOTRON IMPROVEMENT PROGRAMME AND PLANS FOR PHYSICS FACILITIES

E. G. Michaelis
CERN, Geneva, Switzerland.

ABSTRACT

The present status of the CERN SC Improvement Programme is summarized. Details are given of the design and performance of some components incorporating novel features. The beam facilities planned for future physics research are described.

1. INTRODUCTION

The CERN Synchrocyclotron Improvement Programme (SCIP) aims at an increase of the present beam current of about 1 μA by an order of magnitude and of the present extraction efficiency of about 7% by a large factor. Details of the project have been published. References 1 and 2 contain full lists of relevant papers and reports. As similar projects elsewhere [3, 4] SCIP relies on a small-diameter calutron-source in the midplane and on a narrow gap geometry to overcome the space charge limitations and to reduce the large radial amplitudes associated with the conventional open ion sources. A peak dee-voltage of 25-30 kV permits the use of such a source and allows the pulse repetition rate to be raised from the present 54 Hz to 466 Hz. The reduction of betatron amplitudes will make it possible to increase the extraction efficiency. Unlike the Nevis project [4] SCIP retains the weak focusing field of the present SC. The chief technical problem therefore lies in the provision of a high accelerating potential over a frequency band from about 30 to 16.7 MHz. Additional problems are created by the need to avoid any build-up of radial amplitudes due, for example, to incorrect positioning of the source or misalignments of the electrical and magnetic centres, as have been described by Holm [5].

The project was formulated in 1967 by Dr. G. Brianti [6] and authorized by CERN in November 1968.

2.1 THE ACTIVATION PROBLEM

The mechanical design of many elements in and near the main vacuum chamber has been influenced by the expected levels of machine activation. Fig. 2.1.1, due to Barbier, shows the γ dose in rem/h 24 hours after shutdown after prolonged operation with a 10 μA internal beam. The interior of the vacuum tank will be inaccessible and no work requiring more than a few minutes can be performed in its immediate vicinity.

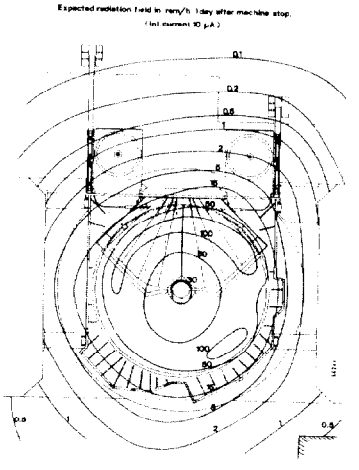

Fig. 2.1.1

We have therefore constructed supports permitting rapid removal and replacement of any element requiring service or repair from the active area. By this construction we shall not only be able to service the machine but also hope to maintain its development potential.

2.2 MAIN VACUUM CHAMBER AND MAGNET

Fig. 2.2.1 shows the principal elements in and near the main vacuum chamber.

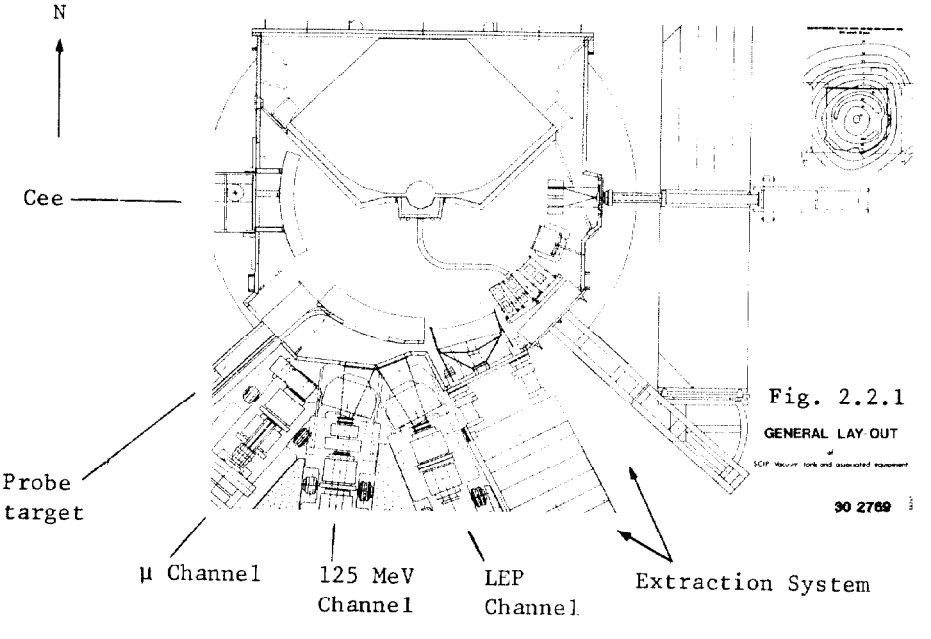

Fig. 2.2.1

- the vacuum tank, shown in plan, is a stainless steel box whose outside surfaces are joined by grooved double welds. Its top and bottom are the pole-faces of the SC magnet. The north wall is formed by the pump-manifold which carries the dee and the liner. The other walls have windows for the beam elements and are shaped so as to facilitate the compression of vacuum seals.

The figure shows :

- the cee-electrode mounted on the west wall, its feeder line passing through a hole in the yoke,

- a port in the south-west corner holding the probe-target, removable so as to permit the passage of the internal target frame,

- windows in the south wall for beams for secondary beams from internal targets and for the electromagnetic extraction channel,

- the port in the south-east corner which, with the aid of a swivelling table, allows removal of the iron-channel, the regenerator and the polarized dummy dee,

- the pulsed field coil attached to the west wall.

The ion source is mounted on a support below the magnet and is introduced via an axial hole. A symmetrical hole in the upper yoke houses the beam-limiter. The rig to be used for cutting these holes has been constructed by industry and is described by Herridge[7].

The axial holes modify the magnetic field at the centre of the machine. Moreover, we require a value of $k \sim 2$ near the centre. Shims to provide the required field and gradient have been calculated by Hedin, using a computer code for fields with axial symmetry[8], and have been checked by 1/10 model measurements.

Other possible modifications of the magnetic field may arise from the replacement of the present pole-face shims - to reduce personnel irradiation during the reconstruction - and the replacement of the main-field coils. The new coils are designed to avoid relative movements between layers by winding the pancakes with two interleaved conductors in which the cooling water flows in opposite directions, the stress between neighbouring conductors being taken up by epoxy potting.

These changes of the magnet configuration necessitate a remeasurement of the magnetic field during the reconstruction. Equipment designed to reduce the duration of this work has been prepared; it includes a Siemens 301 computer which controls the sequence of operations and analyses the data on line. The magnetic midplane, critical because of the small dee aperture, will be located using the method of Abrosimov et al[9].

2.3 VACUUM

The vacuum systems of the main tank and of the rotary condenser are separated in order to guarantee the low partial pressure of hydro carbon vapours necessary to avoid electrical breakdown in the rotary condenser. The main tank is pumped by two diffusion pumps, the rotary condenser by a turbo-molecular pump.

The problem of vacuum seals has been studied by Blin[10]. Metal seals are used wherever possible. Elsewhere it is planned to use O-rings of a radiation-resistant ethylene-propylene polymer, mounted on fixtures permitting their rapid replacement.

The seal between the vacuum tank and the poles is shown in fig. 2.3.1.

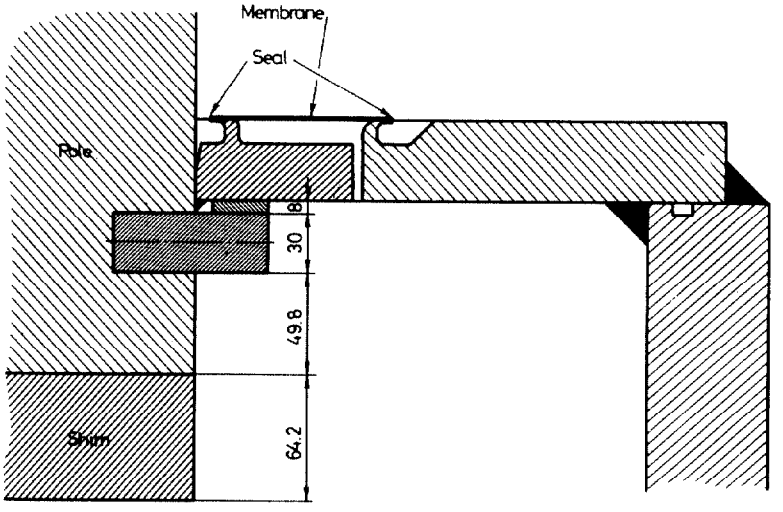

Fig. 2.3.1

It consists of a circular stainless-steel membrane which surrounds the poles and is welded to circular lips. It permits independent movements of the poles and the vacuum chamber. A sample of this seal has been life-tested. Its repair or replacement would be very difficult on account of the radiation problem.

Fig. 2.3.1 also shows the grooved double weld mentioned in section 2.2. The groove is evacuated and facilitates the detection of leaks in the welds.

The vacuum system of the rotary condenser is described in section 2.5 below.

2.4 ION SOURCE AND SUPPORT

There has been no modification in the concept of the ion source and central region previously described [11, 12] but many details have been modified.

Fig. 2.4.1 shows the present design. The conical electrodes are held by boron nitride insulators and are connected to the dee and polarised dummy by bellow-contacts. A trimming condenser is mounted above the electrodes and RF contacts protecting the seals are below them.

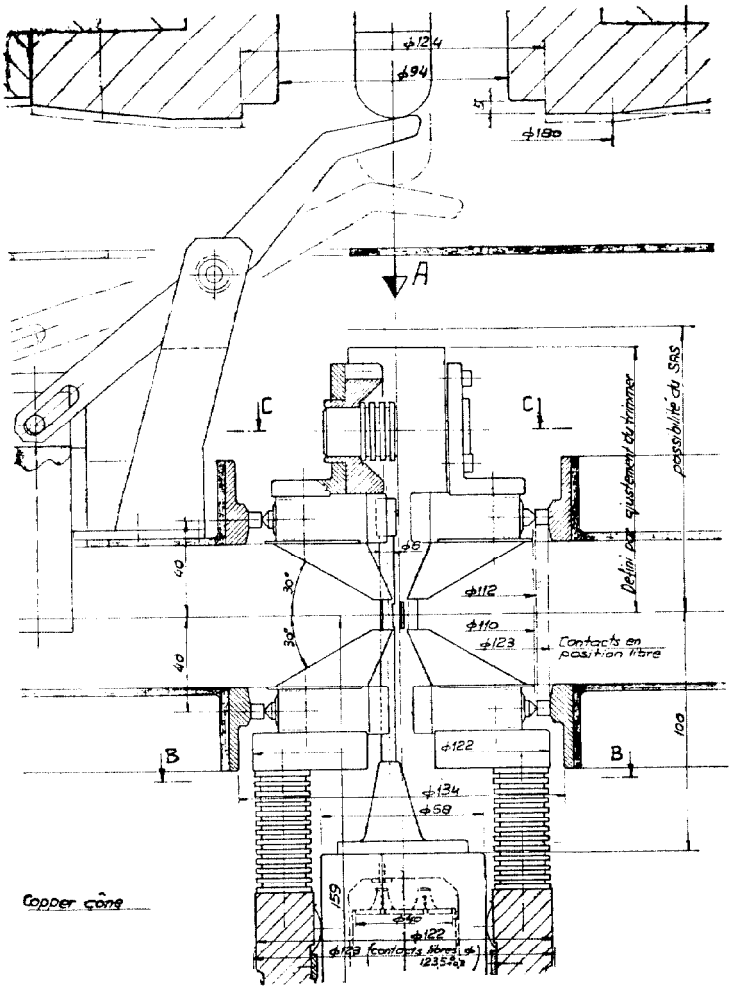

Fig. 2.4.1

To avoid frequent interruptions of operation due to filament failure a feeder system with six filaments has been constructed. By rotating the feeder tube each filament can be placed under the source in turn.

The brilliance of the source is controlled by the adjustment of arc-voltage, arc-current and gas flow. These adjustments can be coupled electronically via a series of function-generators so as to maintain a given brilliance. The "VIG system" performing this operaction has been described by Galiana[13].

The axial support of the ion source and central geometry is shown in figure 2.4.2. It has been designed and described by Bell[14]

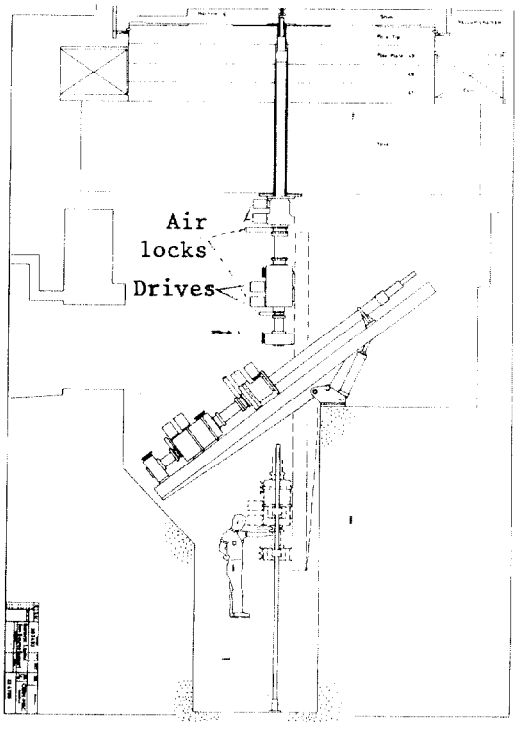

Fig. 2.4.2 Erection column operation detail ion source support

The support consists of six telescopic tubes ranging in diameter from 70 to 180 mm. Tubes of 130 and 70 mm carry respectively the central electrodes and the ion source chimney with the filaments. These tubes are placed eccentrically with respect to the magnet and to each other. With the aid of four stepping motor drives they allow the positioning of the central conical electrodes relative to the dees and of the elements of the source relative to the electrodes. Two separate air-locks provide for the withdrawal of the 130 and 70 mm tubes.

The support is mounted on two vertical columns placed in a 7-metre deep pit below the magnet. A chain drive, locked to the various elements, allows them to be raised and lowered separately.

2.5 THE MAIN RADIO-FREQUENCY SYSTEM

(i) General Characteristics

Information on the design and the main features of the accelerating system can be found in earlier publications [15-18]. Present values of the principal parameters are given in Table I.

TABLE I

Principal Data of the Main Radio-Frequency System

Modulation range	$30.0 - \left(\begin{smallmatrix}17.3\\16.77\end{smallmatrix}\right)$ MHz	Peak accelerating voltage	30 kV
Acceleration time	1383 μs	$(df/dt)_{min}$	-15.65MMHz/ms
Repetition rate	466 Hz		

Adiabatic beam stacking between 16.87 and 17.30 MHz.

Resonator :

$\lambda/2$ capacity loaded, modulated by rotary capacitor, electrical length ≈ 5 m.
Characteristic impedance of matching section : maximum 15 Ω, minimum 3 Ω

Rotary capacitor : 3 rows of 16 teeth.

Outer diameter of rotor	1.44 m	Voltage at minimum gap	18 kV
Rotor speed	1747 rpm	Electrical gap	1 to 4.4 mm
Maximum voltage	46 kV	Capacitance	0.5 to~7 nF

Coupling capacitor to stub :

Constant capacitance	20 nF	Electrical gap	0.3 mm
Current	3.25 to 8.2 kA	Voltage	0.85 to 4.3 kV

Oscillator : Self-excited tetrode, type RS 1041W anode and screen - grid modulated

Variable coupling capacitor to oscillator	Max. ≈ 700 pF	Min.≈ 100 pF
Voltage at oscillator	8 to 12.5 kV)	variable with
Power dissipation	105 to 212 kW)	frequency
Maximum oscillator power	150 kW CW	

Main Dee :

180° to r = 0.6 m.
Cut back by 15° at 0.6, 0.95 and 1.3 m from vertical symmetry plane.
Aperture 60 mm for r < 1.89 m, 120 mm in target region.

Maximum radius	2.35 m	DC bias	~ 2 kV

Polarized dummy dee :

Radius	0.40 m	DC bias	as main dee

The RF system, considered as a non-uniform transmission line, tuned to resonance by a variable shunt capacitor, is shown schematically in Fig. 2.5.1 which also indicates the function of the various elements.

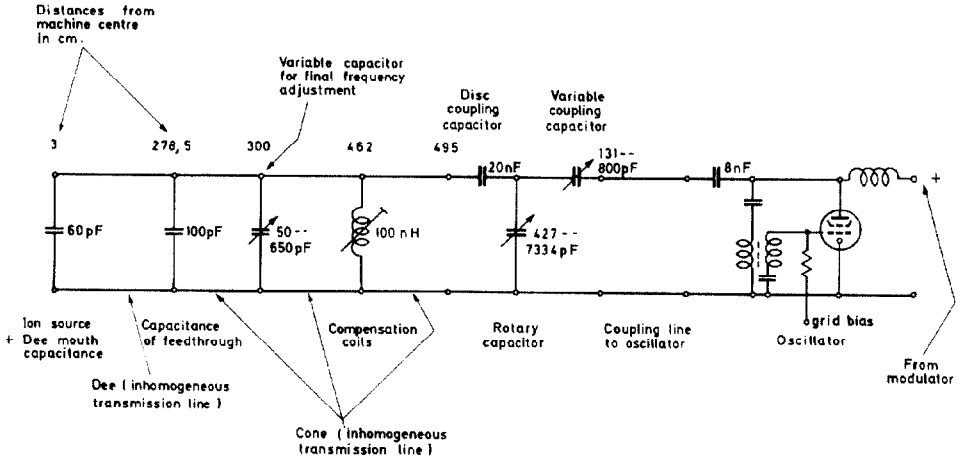

Fig. 2.5.1 Simplified circuit diagram RF system SCIP

The electrical properties of the resonator have been verified by measurements on a 1/1 scale model. The results of this work are summarized by Kanowade [18]. His results as to the voltage and current distribution at different points along the resonator are shown in Fig. 2.5.2 for the two extreme frequencies.

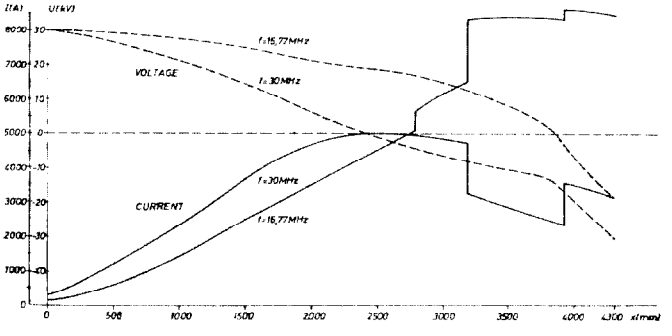

Fig. 2.5.2 Horizontal and vertical cross section of the RF system. Voltage and current at the minimum and maximum frequency. The space coordinate corresponds to the figure above.

The peak power consumption of the system is about 210 kW and occurs at an intermediate frequency, whose value depends on the choice of the final frequency.

(ii) Oscillator and Modulator

The oscillator circuit is indicated schematically in Fig. 2.5.1. It incorporates a wide-band feedback transformer using a ferrite-core; filters for the suppression of parasitic modes are incorporated in the circuit but not shown in the diagram. A voltage modulator, using an RS 567 as series triode, provides for a programmed variation of the oscillator high-tension.

The oscillator valve and the ferrite ring are magnetically shielded in an iron box which also houses the rotary condenser. Additional shielding is provided by two concentric iron cylinders surrounding the valve and transformer. They are silver-plated and form part of the feedback circuit.

(iii) Rotary Condenser

The rotary condenser consists of an aluminium alloy rotor running on a cantilevered shaft between the earthed stator blades. It is driven by a variable speed motor and rotates in vacuum at speeds of up to 2600 revs/min.

The condenser and the conical conductors matching it geometrically and electrically to the dee are shown in section in Fig. 2.5.3.

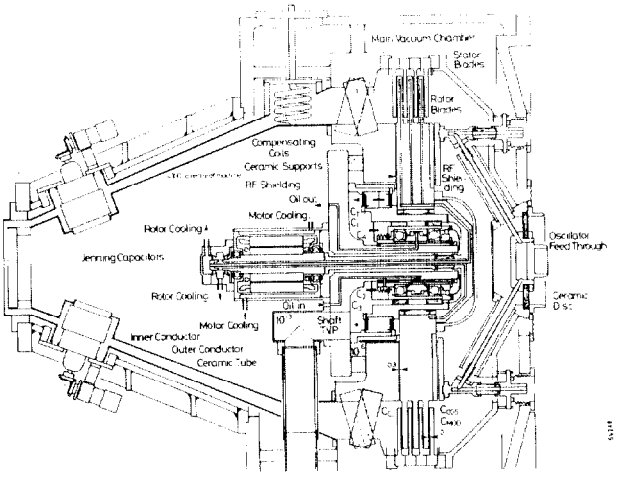

Fig. 2.5.3

The figure indicates the position of the principal elements with the exception of the complicated ducts which carry cooling water, oil, the electrical supplies, bias voltages and control signals through th hollow compensating coils to the rotor motor, support shaft and the ball-bearings.

Both rotor and stator blades are radially tapered. Additionally the stator blades are shaped at their inner edge and azimuthally tapered to provide the required variation of capacity. All blades are water-cooled and are designed so as to avoid mechanical resonant frequencies within the working range.

Fig. 2.5.4 is a view of the rotor and coupling condensor mounted on the support shaft. Four of the 64 stator blades prior to final machining are shown in Fig. 2.5.5.

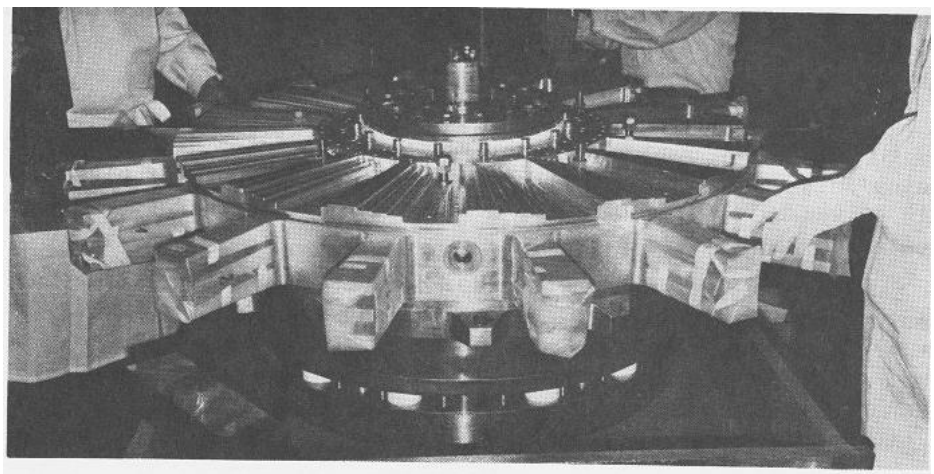

Fig. 2.5.4

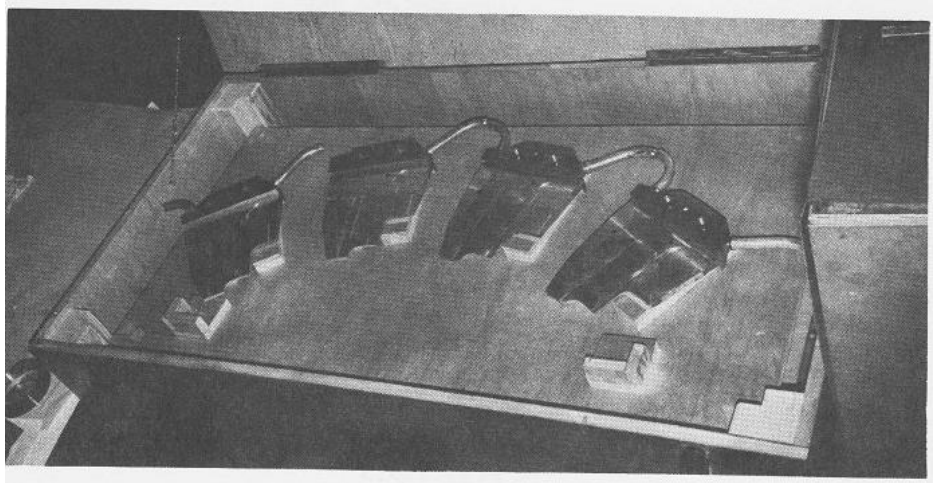

Fig. 2.5.5

The stator blades are held by the outer support ring. Ten aluminium oxide insulators, mounted in this ring, support the inner ring, which, via a further set of insulators, holds the assembly of drive motor and the support shaft of the rotor.

This construction provides the mechanical stability required by the small clearances between rotor and stator blades and in the 0.3 mm coupling condenser to the stem. It also reduces the potential difference across the ball bearings, which are additionally protected by a network of four balanced capacitors. Details of this design and experimental results on bearing life-times under various conditions are to be found in ref. 17.

To reduce the risk of voltage breakdown in the rotary condenser due to oil vapour, the oil lubricating the bearings is retained by a rotary-face seal. Any leakage oil drains into a separately-pumped duct, and a turbomolecular pump mounted on the rotor shaft prevents the flow of oil vapour into the condenser gap.

The entire assembly shown in Fig. 2.5.3 is housed in an aluminium-alloy casing evacuated by a 4000 l/s turbomolecular pump. Aluminium wire seals are used where possible.

Power losses due to eddy currents in the rotor caused by the stray field of the SC magnet are reduced by a magnetic shield. The estimation of these losses is complicated by the shape of the rotor and by the inhomogeneity of the field. Fiebig and Hedin have calculated the losses, taking account also of the skin effect which tends to reduce them[19]. Their results, verified in a 1/10 model, show that the losses will be less than 1 kW for fields below 100 G.

The magnetic shield also houses the oscillator. Both oscillator and rotco are mounted on carriages running on two sets of rails

During operation the rotco is also subject to a flux of 10^7 high-energy neutrons/cm^2.s and will therefore be activated. To reduce down-time necessitated by cooling after a breakdown, two identical condensers will be provided.

The operation of the rotary condenser is controlled by various monitors, of which the most important is an inductive vibration detector, capable of registering amplitudes of 15 μm.

(iv) The Dee System

Fig. 2.5.6, a plan view of the dee, shows the gradual cut-back from 180° at the centre to 90° at full radius. Fig. 2.2.1 shows the dee-dummy-dee gap to be symmetrical to about 1 m radius; this minimizes the effect of the cut-back on the radial amplitudes.

The dee aperture increases from 1.3 cm at the centre to 6 cm at r = 7 cm (see Fig. 2.4.1). At radii above 190 cm the aperture flares out to 12 cm at r = 215 cm.

The stator blades are held by the outer support ring. Ten aluminium oxide insulators, mounted in this ring, support the inner ring, which, via a further set of insulators, holds the assembly of drive motor and the support shaft of the rotor.

This construction provides the mechanical stability required by the small clearances between rotor and stator blades and in the 0.3 mm coupling condenser to the stem. It also reduces the potential difference across the ball bearings, which are additionally protected by a network of four balanced capacitors. Details of this design and experimental results on bearing life-times under various conditions are to be found in ref. 17.

To reduce the risk of voltage breakdown in the rotary condenser due to oil vapour, the oil lubricating the bearings is retained by a rotary-face seal. Any leakage oil drains into a separately-pumped duct, and a turbomolecular pump mounted on the rotor shaft prevents the flow of oil vapour into the condenser gap.

The entire assembly shown in Fig. 2.5.3 is housed in an aluminium-alloy casing evacuated by a 4000 l/s turbomolecular pump. Aluminium wire seals are used where possible.

Power losses due to eddy currents in the rotor caused by the stray field of the SC magnet are reduced by a magnetic shield. The estimation of these losses is complicated by the shape of the rotor and by the inhomogeneity of the field. Fiebig and Hedin have calculated the losses, taking account also of the skin effect which tends to reduce them[19]. Their results, verified in a 1/10 model, show that the losses will be less than 1 kW for fields below 100 G.

The magnetic shield also houses the oscillator. Both oscillator and rotco are mounted on carriages running on two sets of rails.

During operation the rotco is also subject to a flux of 10^7 high-energy neutrons/cm^2.s and will therefore be activated. To reduce down-time necessitated by cooling after a breakdown, two identical condensers will be provided.

The operation of the rotary condenser is controlled by various monitors, of which the most important is an inductive vibration detector, capable of registering amplitudes of 15 μm.

(iv) The Dee System

Fig. 2.5.6, a plan view of the dee, shows the gradual cut-back from 180° at the centre to 90° at full radius. Fig. 2.2.1 shows the dee-dummy-dee gap to be symmetrical to about 1 m radius; this minimizes the effect of the cut-back on the radial amplitudes.

The dee aperture increases from 1.3 cm at the centre to 6 cm at r = 7 cm (see Fig. 2.4.1). At radii above 190 cm the aperture flares out to 12 cm at r = 215 cm.

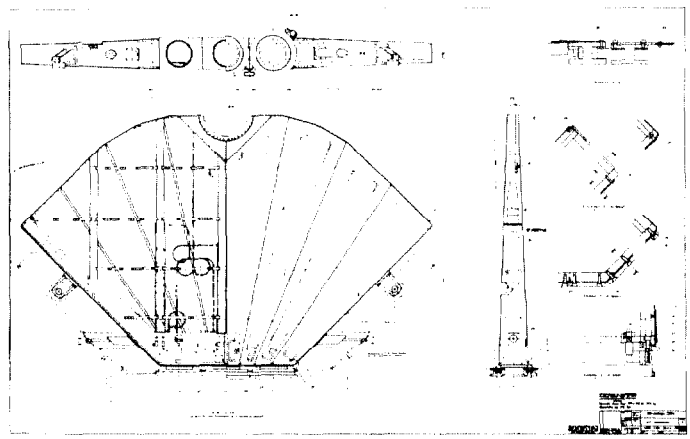

Fig. 2.5.6

A central cut in the dee serves to suppress cross-modes. At r = 20 cm this cut ends in a semi-circular slot which surrounds the central region and is bridged by resistors. The dee is covered with copper-plated aluminium sheets incorporating roll-bond cooling ducts. The skin is supported by pre-stressed girders, indicated in the left half of Fig. 2.5.6 above. Two insulators carry the structure, which is attached to the pump manifold.

Orbit studies performed by Skarek showed that some parts of the dee would be struck preferentially and heated by protons scattered in the internal targets. To avoid any resulting distortion of the dee four of the girders were increased in size and water-cooled. They will act as beam-catchers for scattered particles.

A dee-liner is provided between the pump manifold and the pole pieces with which it is in contact. The pole faces are copper-plated and constitute the remaining liner. The central part of the dummy-dee consists of two semi-circular electrodes, polarized to dee-bias potential. Calculations and experiments have shown that this device avoids a growth of radial amplitudes due to the dee-bias.

2.6 CEE SYSTEM

The peripheral cee is designed to produce a long burst by a slow, secondary acceleration of the beam onto an internal target or into the extraction system.

The principal characteristics of the Cee System are listed in Table II.

TABLE II

Characteristics of the Cee System

Dimensions of Cee			
Angular width:	45°	Radial width: 20 cm	Aperture: $\leqslant$12 cm
Stacking radii:	2.15 - 2.25 m	Peak voltage at gap:	19.4 kV
Modulation range:	160 kHz	Tuning range:	16.77 - 17.48 MHz
Power consumption:	~100 kW	Installed power:	200 kW

The cee operates in single sweep; its bucket area is such as to permit the capture of the entire beam accelerated by the Dee and stacked adiabatically.

The cee is fed by a 200 kW wide band transmitter, employing a 4 CW/100,000 E Eimac Tetrode, via a triple-tuned coaxial resonator of 20 m length.

The principle of the resonant feeder line is illustrated in Fig. 2.6.1. Fig. 2.6.2 shows the input voltage and current for a 19 kV peak output as function of frequency.

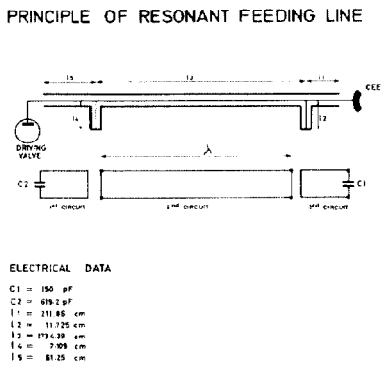

Fig. 2.6.1

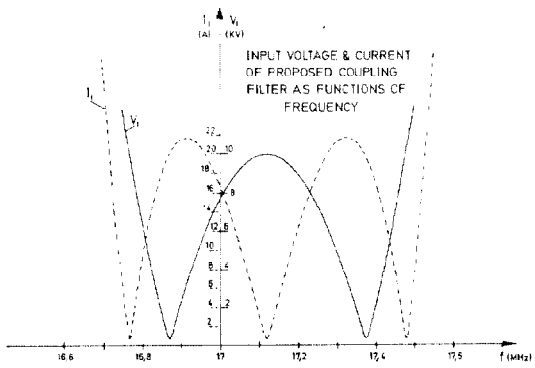

Fig. 2.6.2

A master generator furnishes the frequency and amplitude-modulated RF signal which, after amplification, feeds the output stage. This stage is grid modulated for flattening the response of the coupling resonator and plate-modulated to reduce the anode dissipation.

The cee is expected to provide a beam with 8 to 15% overall duty cycle.

2.7 PULSED FIELD COIL

The pulsed field coil (PFC) is intended to provide a stretched extracted beam free from RF structure by a gradual displacement of the stored internal beam into the regenerator. The theory of its action has been given by Lindbäck[20] and Mandrillon[21].

The PFC is placed close to the regenerator. Table III gives its principal data, supplied by Susini[22].

TABLE III

Pulsed Field Coil Data

Radial position:	2.245 m	Number of turns:	2 x 2
Radial width:	0.2 m	Azimuthal length:	0.5 m
Aperture:	0.12 m	Inductance:	6 μH
Resistance:	≈3 mΩ	Central field:	50 G.m/1000A mean current

The PFC is supplied by a saw-tooth generator shown in simplified form in Fig. 2.7.1.

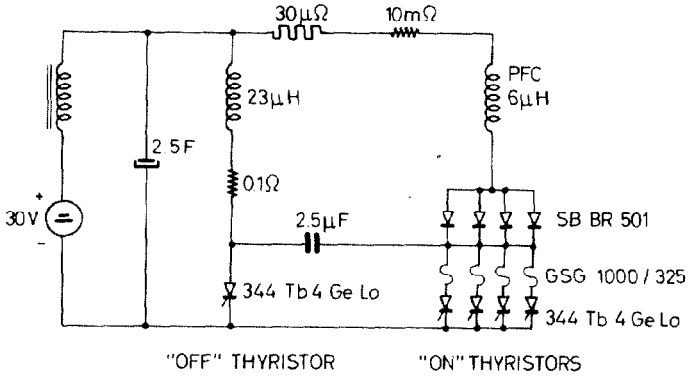

Fig. 2.7.1 PFC Saw Tooth Generator

The current in the PFC rises approximately as

$$i = io\ (1 - e^{-t/\tau})$$

while the "on" thyristors are conducting. They are switched off by the "off" thyristor via the 2.5 F condenser, which causes the coil current to rise and then decrease sinusoidally.

Variants of this circuit employ two exponentials and a biasing current in the PFC. Fig. 2.7.2 shows the field produced under these conditions.

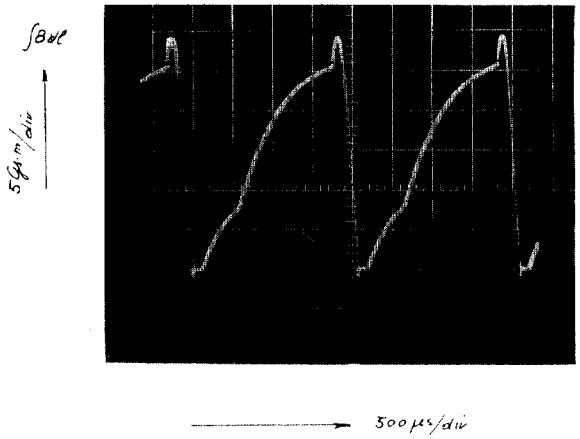

Fig. 2.7.2

Ianovici and Lindbäck [23] have calculated the duty cycle obtainable in the extracted beam, assuming a Gaussian energy distribution of the stacked beam. With various possible pulse shapes in the PFC overall duty cycles from 30 to 70% are obtainable.

2.8 EXTRACTION SYSTEM

The concept of the proposed extraction system has been described by Lindbäck [24]. The system consists of a regenerator, an electro-magnetic channel (EMC) and an iron channel split into three sections. Lindbäck showed that the present poor extraction efficiency of the CERN SC could be accounted for by the radial amplitude of about 10 cm, the septum of 7 mm thickness and the over-focusing produced by the regenerator and the perturbed field in the vicinity of the present channel.

The new design foresees a weaker regenerator. The EMC, consisting of a 3 mm septum, an anti-septum and a compensating system of conductors, has a stray field less than 20 G and a gradient of less than 20 G/cm in the region of the penultimate orbits. The shimming of the iron channel has been calculated by Hedin and Ianovici, who have shown that the beam will not enter the region of rapid field fall-off before extraction.

Fig. 2.8.1 overleaf gives a view of the EMC and of its supporting flange together with the bellows which allow radial adjustments. A 14 kA power supply for the EMC has been constructed by industry.

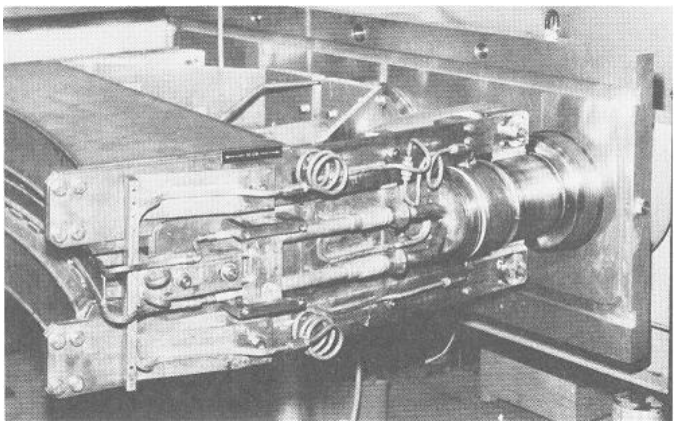

Fig. 2.8.1

Table IV summarizes the principal data of the different sections. ⟨B⟩ indicates the field reduction.

TABLE IV

Extraction Channel Data

Section No.	Length (cm)	Aperture (cm)	P (cm)	⟨B⟩ (G)	$\frac{dB}{dr}$ (G/cm)	Azim.	Adjustment (cm)	Comments
EMC	100	>3.5	245	1860	≈+ 20	7°–31.5°	±1	Remote adj. of entr/exit indep.
1	30	4	275	2200	+350	Entr. 34°	Entr. 1,8	Manual adjustment. Moving as one piece.
2	30	4	275	3200	+300	Exit $\approx 48^{\circ}$	Exit 1,8	
3	54	5.5	350	3900	+700	Exit $\approx 61^{\circ}$	Entr. 1,8 Exit 1,8	Remote adjustment of exit
REG	40	-	∞	-		70°	±2.0	Remote adjustment of rad. pos.

The remote adjustment of the third section of the iron channel will be used to direct the beam to a given exit point.

2.9 INTERNAL TARGETS

The decision to retain internal targets was taken early in the development of the project in view of the existing experimental facilities and of the efficiency and versatility of these targets. However, their use in an improved SC has raised complex problems.

To supply the secondary channels with mesons of various energies the target has to be movable both radially and azimuthally. In addition an axial movement is necessary for beam-sharing. The efficiency of the targets produces high temperatures, but the requirement of mobility permits only radiation cooling. Beryllium is the preferred target material on account of its high secondary yield but cannot be used at temperatures above 1100°K. As a result there is a minimum target size which, in turn, has to be compatible with the acceptance of the beam channels.

This complex of questions has been studied, principally by Bell [25, 26] and Skarek [27, 28]. Part of the study was undertaken by the Ion Physics Corporation, who also designed and tested the target drive.

In the present design four 10 cm long and 1 cm high beryllium targets are mounted on separate trolleys, each of which permits independent movements in three dimensions, actuated by linear motor drives. The four trolleys are mounted on a target frame and can be withdrawn with it from the vacuum tank through the port described in section 2.2. Fig. 2.9.1 is a section of the target frame and trolleys; one of the target trolleys carrying a target is shown in Fig. 2.9.2.

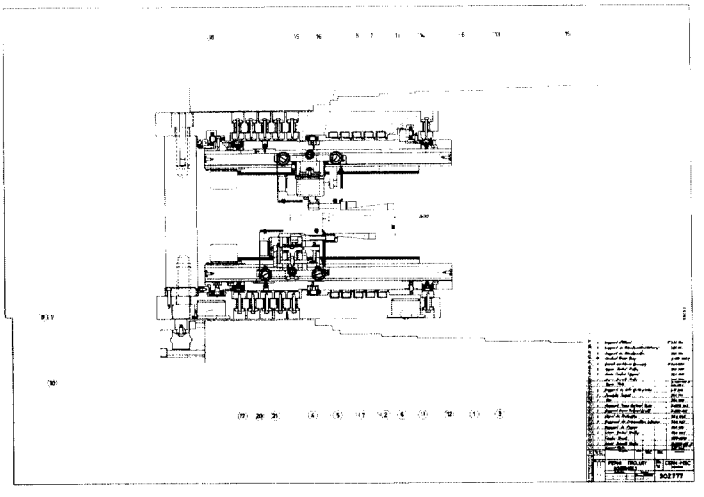

Fig. 2.9.1

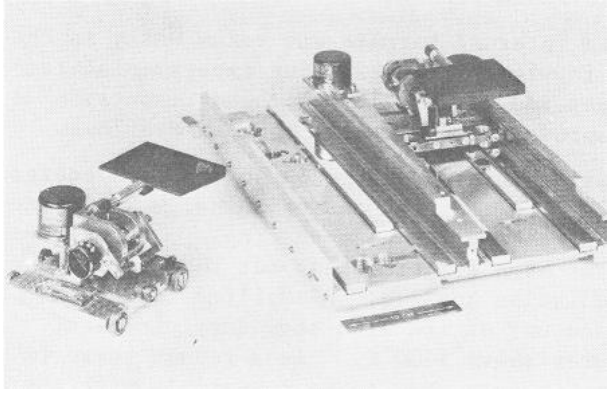

Fig. 2.9.2

The movements of these targets and the contacts necessary to supply the linear motors have been tested. A maximum current of 60 A is required for azimuthal positioning.

A probe target will be provided for target irradiations and beam diagnostics; it will be mounted on the platform which serves for the withdrawal of the target frame. Its design is in progress.

2.10 SHIELDING

Reinforcements of the shielding, necessary to maintain the stray radiation in the experimental halls at about the present level, have been calculated by Barbier and Tommasini[29] who recommend the use of solid iron shielding in the beam plane sections of the proton and neutron side shield walls. Regions of high neutron flux are to be reinforced with a special shielding material of high density and high hydrogen content (Chemtree 26) to attenuate the flux of neutrons of energies below 15 MeV.

Rotary vacuum beam-blockers, consisting of 1 m diameter iron discs, are integrated in beam trolleys which carry the beam transport and collimators of the pion beams from internal targets.

3. EXTERNAL BEAMS

The external beam systems of the CERN SC are indicated schematically in Fig. 3.1. Secondary beams from the internal targets are directed to the Neutron Hall; secondary beams from the external target point T go to the Proton Hall and the full extracted proton beam U goes into the Underground Experiment Area which houses the on-line isotope separator. The future beams are described in a recent report by Cox et al [30] and only a summary will be given here.

Table V lists the characteristics of the beams; Table VI gives estimates of particle flux and energy spread. All beams are variable in energy.

As an illustration of the redesigned secondary beam from an external target the D-beam is shown in Fig.3.2. It consists of two spectrometers of which the first produces a dispersive and the second an achromatic image of the target. By placing a collimator or hodoscope at the first image it should be possible to reach an energy resolution of about 0.2% within a 2% energy band.

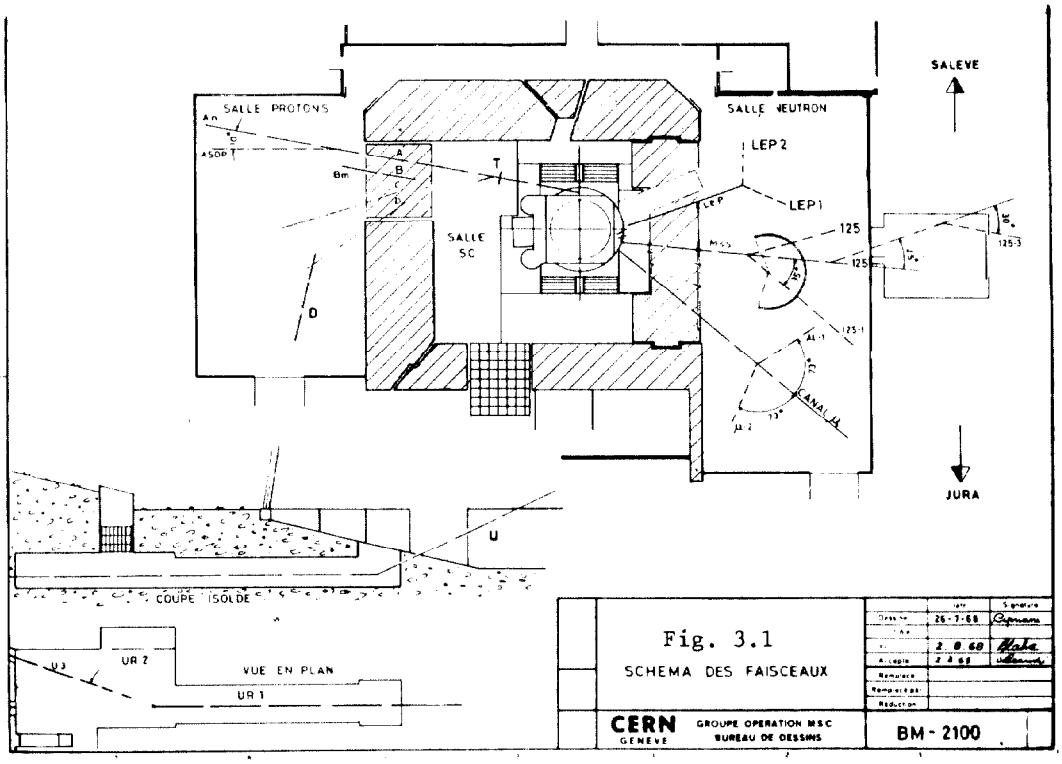

Fig. 3.1
SCHEMA DES FAISCEAUX

TABLE V

Characteristics of the Beams

Hall	Beam	Particles	Characteristics
N	LEP	π^+, π^-	Low resolution, low energy
	125	π^-	High resolution, intermediate energy
	μ	μ^-, π^-	Low resolution, low and high energy
P	B	π^+, π^-	Low resolution, high flux
	C	π^+, π^-	Medium resolution, high flux
	C	n	Resolution given by production target
	D	π^+, π^-	High resolution, low flux

TABLE VI

SC 2 EXTERNAL BEAMS

Hall	Target	Beam	Particle	Energy Range (MeV)	Total Flux s^{-1}	Beam Characteristics at Energy (MeV)	ΔE[b] (MeV)	δE[c] (MeV)	Spot Size cm^2	Stop Rate $g^{-1}s^{-1}$
N[a]	int.	LEP	π^+	60 - 105	10^6	85	7		10	1.4×10^4
			π^-	60 - 105	5×10^6	90	7		10	4×10^4
		MSS	π^-	110 - 260	3×10^6	180	10	<1	3	
		μ	π^-	110 - 170	10^7	127	17.5		40	6×10^3
			μ^-	50 - 190	5×10^5	56	11		100	2×10^3
P[a]	ext.	B	π^+	100 - 284	2×10^8	284	47		36	
					5×10^7	104	28		"	
			π^-	100 - 284	2×10^7	280	47		"	
					1×10^7	104	28		"	
		C	π^+	100 - 413	10^6	413	1.4		< 20	
					4×10^6	365	1.0		"	
					3×10^8	275	5		"	
					5×10^7	104	12		"	
			π^-	100 - 284	3×10^7	280	25		"	
					5×10^7	190	19		"	
					1.5×10^7	104	12		"	
		C	n	400 - 600	6×10^6	600			≈ 75	
		D	π^+	100 - 284	2×10^7	275	5.0	0.36	< 1	
					10^6	104	2.4	0.19		
			π^-	100 - 284	6×10^5	284	6.0	0.36		
					2×10^5	104	2.4	0.19		
U		U3	p		$\geq 3 \times 10^{13}$	600	0.5			

(a) N beams are calculated for 10 μA internal beam current, P beams for 5 μA extracted current on an external target.

(b) ΔE = Energy spread in beam. (c) δE = Energy resolution.

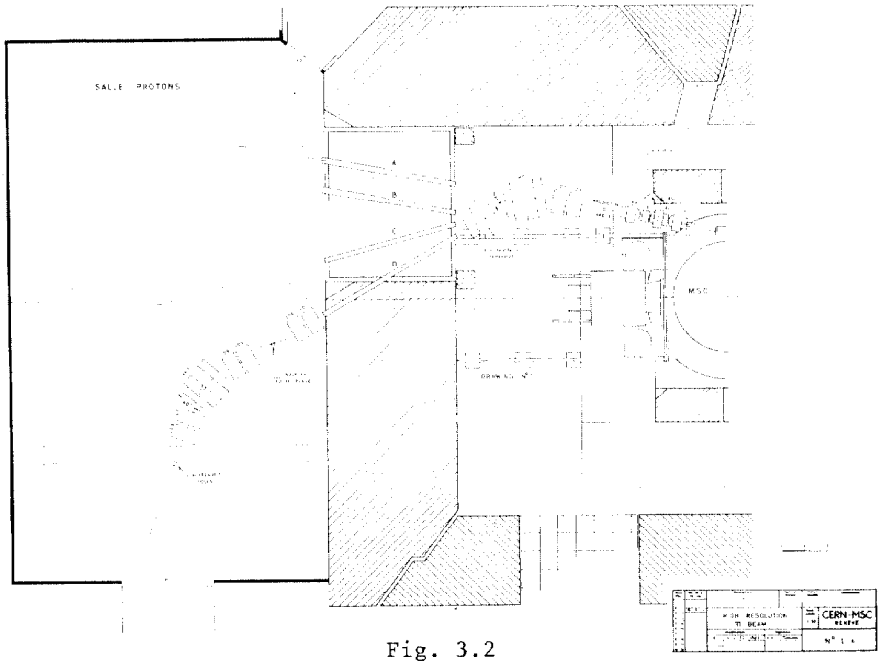

Fig. 3.2

The second spectrometer, which is mounted on a carriage can also be used as part of the detection system by rotating it about a target placed at the first image.

The beam provides space for an electrostatic separator which will be necessary to eliminate the large flux of degraded protons.

4. PRESENT STATUS

Since the start of the work early in 1969, the project has suffered a delay of about one year due to difficulties encountered in the manufacture of the rotary condenser by industry. The resulting postponement of the shutdown has, however, enabled us to advance many other jobs with the aim of shortening the time required for their installation.

At the time of writing (July, 1972) many elements of the project have been completed or are under test, notably

- all building modifications
- the new main field coils
- the drilling rig for the yoke
- the extraction channel and its power supply
- the cee and its main amplifier
- the pulsed field coil and sawtooth generator
- the ion source support
- the vacuum chamber

- the dee and pump manifold
- the oscillator of the main RF system
- the magnetic shielding for rotor and oscillator

Many other items are in an advanced state of construction, e.g. the target system, the neutron-side meson beams and the supports for the various beam elements in the vacuum tank. Detailed plans have been prepared for the installation during the shutdown of cables and new cooling supplies.

The rotary condenser has undergone its mechanical tests. Its final assembly with vacuum tests at each stage is in progress in preparation for a full-power electrical test of the entire radio-frequency system.

5. ACKNOWLEDGEMENTS

The work described has been performed by many past and present members of the MSC Staff, the MSC Group Leaders - H. Beger, F. Blythe, G. Le Dallic and N. Vogt-Nilsen - taking primary responsibilities, as did M. Lažanski until March, 1971.

The writer's thanks are due to R. A. Bell, J. J. Domingo, A. Fiebig, B. Hedin, P. Mandrillon and G. Spinney for help in the preparation of this paper.

REFERENCES

1. MSC Staff, Proc. 5th Int. Cyclotron Conf., Oxford, 1969, p. 719.
2. Michaelis, E. G. MSC-M-6 (1972).
3. Synchrocyclotron Group, Harwell, Proc. 5th Int. Cyclotron Conf., Oxford, 1969, p. 673.
4. Cohen, R. et al., Proc. 5th Int. Cyclotron Conf., Oxford, 1969, p. 699.
5. Holm, S. Proc. 5th Int. Cyclotron Conf., Oxford, 1969, p. 736.
6. Brianti, G., MSC Int. Rep. 67-6 (1967).
7. Herridge, F. W., Machinery and Production Engineering, No. 3102, vol. 120, 575 (1972).
8. Hedin, B. MSC Int. Rep. 71-7 (1971) and Proc. Conf. on Magnet Technology, Stanford (1965), p. 89.
9. Abrosimov, N.K., Eliseev, V. A. and Ryabov, G. A. A. F. Joffe Physico-Technical Institute Report No. 40, (1967).
10. Blin, A. MSC-M-20 (1970).
11. Galiana, R. Proc. 5th Int. Cyclotron Conf., Oxford, 1969, p. 728.

12. Comiti, S. and Galiana, R. CERN Rep. 70-9 (1970).

13. Galiana, R. MSC/PR/584, Source du SC 1, 19.2.70.

14. Bell, R. A. MSC-M-16 (1971).

15. MSC Staff. MSC Int. Rep. 67-5 (1967).

16. Hecken, R. and Talas, S. MSC-M-35 (1968).

17. Beger, H. H. IEEE Trans. Nucl. Sci., NS 18, 307 (1971).

18. Kannowade, H. H. IEEE Trans. Nucl. Sci., NS 18, 315 (1971).

19. Fiebig, A. and Hedin, B. Private communication (1971).

20. Lindbäck, S. IEEE Trans. Nucl. Sci., NS 18, 328 (1971) and MSC-71-1 (1972).

21. Mandrillon, P. Thesis, Univ. Grenoble, 1971.

22. Susini, A. Private communication, 1972.

23. Ianovici, M. and Lindbäck, S. MSC Int. Rep. 72-1 (1972).

24. Lindbäck, S. Proc. 5th Int. Cyclotron Conf., Oxford, 1969, p. 235.

25. Bell, R. A. MSC-M-3 (1970).

26. Bell, R. A. MSC-M-19, (1971).

27. Michaelis, E. G. and Skarek, P. Nucl. Instr. Meth., 89, 81 (1970).

28. Skarek, P. MSC-M-3, (1970).

29. Barbier, M. and Tommasini, T. MSC-M-10 (1970).

30. Cox, C. R., Domingo, J. J. and Skarek, P. MSC-M-1, (1972).

DISCUSSION

RICHARDSON: I noticed that you have a variable input coupling capacitance. Does this give you a fairly constant dee voltage with time?

MICHAELIS: We are aiming at a dee voltage which is, in fact, strictly constant in time and equal to about 30 kV peak input coupling. The variable condenser is supposed to give a more or less constant output impedance to the oscillator.

RICHARDSON: My second question was the variation of frequency with time.

MICHAELIS: We have to sweep through a range of 13 Mc in the order of 1.3 msec.

RICHARDSON: But you and I know that performance depends upon that variation of frequency with time. Is it under your control?

MICHAELIS: It is under our control. The stator blades are shaped in such a way that we get essentially a slowly-rising bucket. We have not yet cut the blades to their final shape. They have been tapered but we left ourselves a reserve of material so that we have a way of approaching the final frequency programme. We can't control it by turning a button, but we can make it so that it suits us. There is also an additional control of the bucket size in that the high voltage can be programmed. If the frequency programme is somewhat wrong, we can correct the bucket error by modulating the accelerating voltage during the course of the acceleration.